Observation of Large-Delta-Magnitude Close Binaries with Shaped Aperture Masks

Edward L. Foley[1], Russell M. Genet[2], John R. Ridgely[1], David Rowe[3], and Neil T. Zimmerman[4]

1. California Polytechnic State University, San Luis Obispo
2. Orion Observatory, Santa Margarita, California
3. PlaneWave Instruments, Rancho Dominguez, California
4. Princeton University, Princeton, New Jersey

Abstract In this paper, the motivation, history, mechanism of operation, and practical usage of shaped aperture masks are discussed in the context of binary star observation and discovery.

Introduction

Binary star systems are important subjects for astronomical study. Records of star separations and position angles, taken over a number of years, allow us to establish orbits and calculate the dynamical mass of binary systems via Kepler's Third Law. The dynamical mass, when coupled with other information, yields the mass of each constituent star, the single most sensitive parameter affecting stellar evolution. In close pairs with a large brightness difference, the light from the brighter star often overwhelms the light from the dimmer star. The faint stars are thus difficult to isolate, and so they are relatively under-observed.

Many of these overlooked stars are late-M stars, which are cool, faint, and red (Figure 1). The charge-coupled device (CCD) cameras used to observe these stars has low sensitivities at red wavelengths where late-M stars radiate the most energy, further exacerbating the problem (Figure 2). Recent adaptive optics (AO) observations of late-M stars showed that some mass estimates were off by a whopping factor of two or more (Dupuy et al. 2010). With accurate speckle observations and orbital analyses of a larger number of short-period binaries with late-M secondaries, we can refine our stellar evolutionary models and strengthen the conclusions we draw from them. First, however, we must discover these stars!

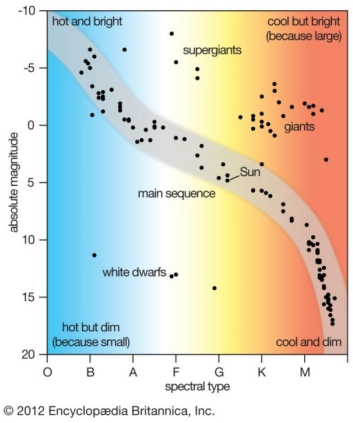

Figure 1. The Hertzsprung–Russell diagram (Encyclopædia Britanica). We are most interested in the late-M secondary stars that appear in the lower-right of the diagram.

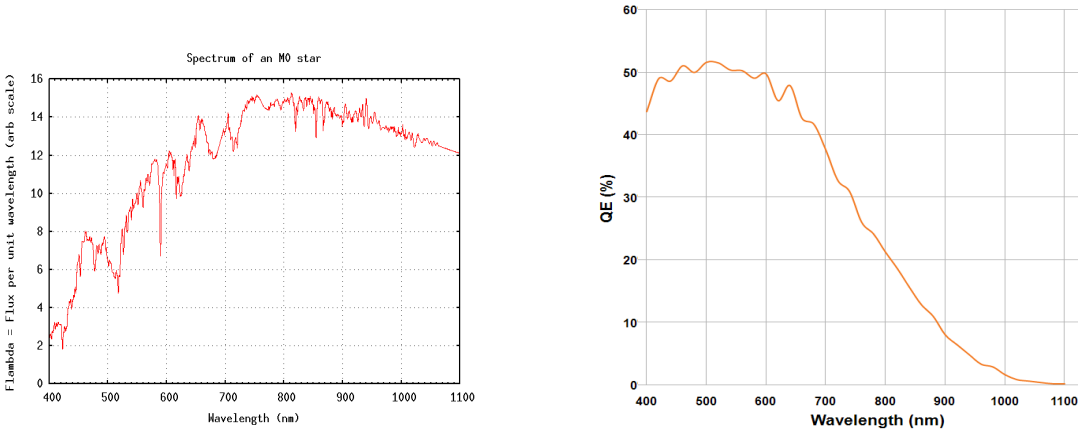

Figure 2. A typical spectrum of an M0 star (left) compared to a typical CCD sensitivity profile (right) ("Andor Luca-S 658M Specifications"; Richmond 2011). This star has significant energy output at wavelengths longer than 800 nm. The camera's sensitivity is low in this range, though the camera can still detect infrared light.

Shaped aperture masks and shaped pupil masks are innovative solutions to the double-star, large-delta-magnitude problem, and have been used successfully in practice (Debes et al. 2002; Debes & Ge 2004, Daley 2014). The masks' strategically-shaped contours diffract light in such a way that the light destructively interferes with itself in prescribed image regions. These regions, known as *discovery zones*, provide exceptional contrast. Astronomers can use this contrast to their advantage: if a telescope is centered on the primary star of a double-star system, the light from the bright primary will disperse about the image, leaving the discovery zones largely unaffected and facilitating the detection of any faint companion stars therein.

Modern pupil masks are proposed for use in exoplanet discovery and observation because of the extremely high contrast requirements of this area of research. Host stars can outshine hot Jupiters by factors exceeding 10^6 and Neptunes by factors around 10^9 (Kasdin 2014). Consequently, aperture masks must be designed with great care and machined precisely to allow such observations to take place. The inherently high contrast ratio requirements surrounding exoplanet study are an expensive barrier to entry. Luckily for smaller observatories, there is a considerable amount of science that can be performed on binary stars at more modest contrast ratios closer to 10^3—ratios that may be possible to attain without specialty equipment. Further, small, ground-based telescopes have easily accessible apertures near which a mask can be placed, as opposed to larger telescopes with available pupils further down the optical path. The terms s*haped aperture mask* and *shaped pupil mask* imply different placements, but the masks' functions are identical.

Speckle interferometry can be used with shaped masks to resolve regions within the atmospheric seeing limit; thus, these masks are theoretically capable of distinguishing stars that simultaneously have large delta magnitudes and small angular separations. There is much to learn from binary stars with magnitude differences between 3.0 and 8.0 and angular separations near the seeing limit (less than a few arc seconds). Shaped masks may enable small observatories to study stars meeting these criteria. For the same distance from Earth, more closely spaced binaries have shorter-period orbits, meaning star motion can be tracked over a shorter timeframe to arrive at meaningful orbits and mass estimates. Adaptive optics systems can be used in large observatories to replace the speckle process, but the system's higher cost is not a realistic investment for some astronomers.

The shaped masks that can be readily manufactured have azimuthally-limited discovery zones. This is not an issue during observation where the approximate position of the secondary star is known, but when it is not—as in the case of binary star discovery—one must repeatedly rotate the mask to survey the primary star's surroundings. For example, if a symmetric mask has 20 degrees of visibility on each side,

it has a 40-degree discovery window and must be positioned in at least nine different orientations to completely scan the 360-degree neighborhood of a primary star. In practice, each new discovery zone should slightly overlap the previous to avoid problems when the secondary happens to fall on a discovery zone border. Manual realignments would be slow and tedious, making the rotation of shaped masks an ideal target for automation.

Other Approaches

While we concentrate in this paper on the use of shaped aperture masks to disperse the light from the bright primary star away from a discovery zone for secondary stars, there are other approaches that have been or could be taken to observe close binary stars with large delta magnitudes. Below we discuss occulting bars, photometric systems, and Lyot stops.

Occulting Bars

One simple method of shielding dimmer stars from brighter companions is to use an occulting bar (or "dot"). Occulting bars are strips of highly-attenuating or opaque material placed at the focal plane. When this strip is aligned with the brighter star in the image, that star's light is diminished or blocked entirely within the region covered by the strip. See Figure 3 for an example.

Figure 3. Aluminum foil occulting bar applied to an eyepiece (Sinnott & Ashford 2005).

The construction of occulting bars needs not be precision science: hobbyists on online forums have used aluminum foil, toothpicks, wire, and other readily-available materials to good effect. The goal is to produce a crisp edge in the image, but this can be difficult to obtain when the occulting material has rough edges or is placed away from the plane of focus (Sinnot and Ashford 2005). Securing these materials without damage to the telescope optics can be a daunting task (Daley 2014).

The simple construction and operational principle of occulting bars are attractive, but the occulting method becomes ineffective when applied to close binaries. Because the strip attenuates only the most direct light but does nothing about halos from bright stars, light from dim secondaries can still be overwhelmed, even when the telescope is perfectly aligned. Worse, the jitter of atmospheric seeing prevents continuous perfect alignment: depending on the arrangement of the visual cell artifacts at any moment, primary light may escape the occulted region or secondary light may enter it.

Shaped masks do not have this problem because they have the power of spatial convolution on their side. As explained further in the "Shaped aperture masks" section, the diffraction patterns caused by telescope apertures will appear *locally* at each point of light. Effectively, shaped masks perform their function without regard to light position. Occulting bars, on the other hand, are highly sensitive to light position.

Photometric Systems

Photometric systems employ filters that transmit light over only a particular range of wavelengths. For example, a filter designed to exclusively transmit infrared light would attenuate or remove shorter-wavelength visible light. The transmission profile of this filter would resemble that of Figure 4. This filter would allow better visibility for secondary stars emitting light at longer wavelengths if they are coupled with primary stars emitting light at shorter wavelengths.

Infrared-pass filters remove a significant portion of the light at the wavelengths that CCD cameras are most sensitive to (see Figure 5); thus, while the filters are effective at emphasizing red stars over blue stars, the amount of usable light is reduced dramatically. The combined effect of the infrared filter of Figure 4 and CCD sensitivity profile of Figure 5 is shown in Figure 6 for two stars: a 10,000-kelvin A-type star and a 3,000-kelvin M-type star.

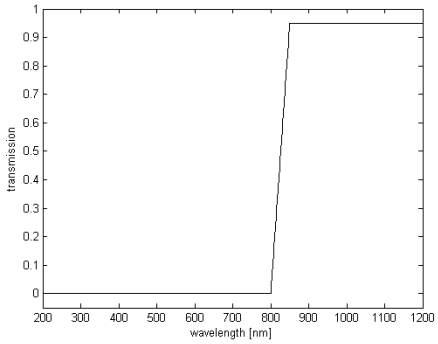

Figure 4. Example transmission profile of a filter designed to transmit infrared light.

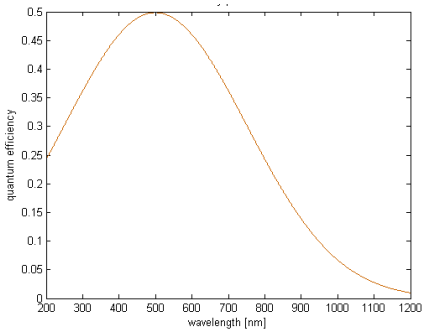

Figure 5. Approximate sensitivity profile of a CCD camera, modeled as a Gaussian distribution. Compare with Figure 2.

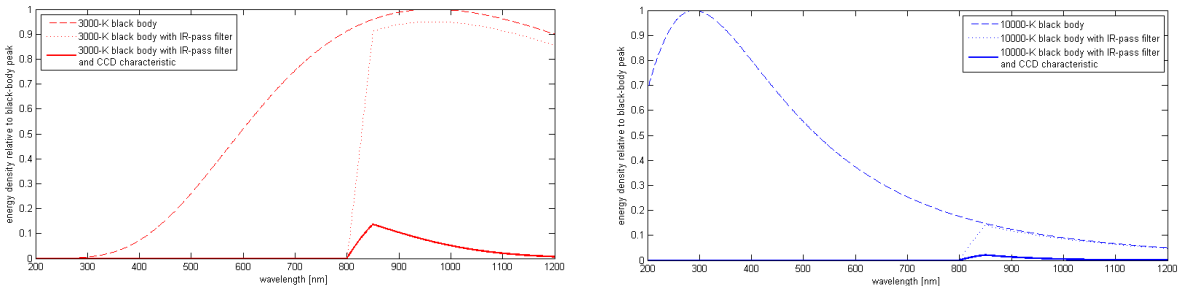

Figure 6. The effects of an infrared filter and CCD transmission profile on a 10,000-kelvin black body (right) and a 3,000-kelvin black body (left). Note how the combination of the IR-pass filter and poor CCD sensitivity removes nearly all of the original energy from the 10,000-kelvin star but not the 3,000-kelvin star.

When applied to binary systems with significantly dissimilar spectral classes, photometric systems can be effective and relatively inexpensive. They also benefit from the ability to be combined in series with other equipment such as occulting bars and shaped masks. Of course, the usefulness of photometric systems is limited when stars have nearly the same color.

Lyot Stops

Lyot stops are masks that are shaped to block unwanted diffracted light caused by some obstruction in the optical train. In the context of coronography, this obstruction is typically a central occulting dot that is intended to block primary light at the center of the field of view. The dot causes a diffraction pattern whereby the central light is effectively relegated to a circular fringe. The Lyot stop then blocks a large portion of this fringe. The net result is highly attenuated primary light and high contrast for off-axis elements such as stars and exoplanets. This process is diagrammed in Figure 7.

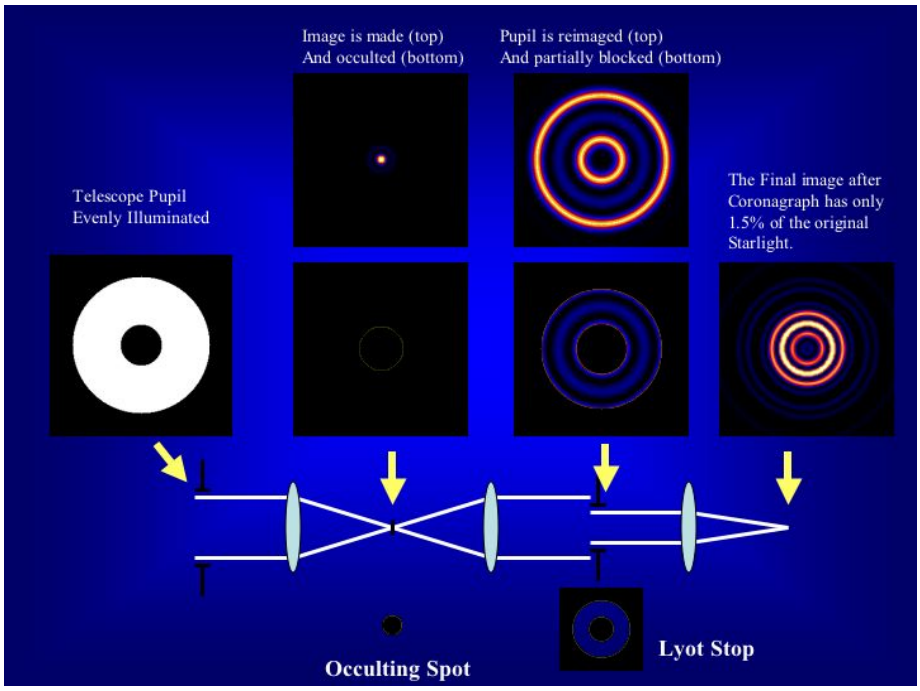

Figure 7. An overview of Lyot stops' mechanism of operation (Oppenheimer 2003, adapted from Sivaramakrishnan et al. 2001).

Lyot stops fall victim to the same problems that occulting bars have: they cannot guard against atmospheric seeing effects themselves. Instead, an expensive adaptive optics system is required to reverse the atmospheric distortion and keep light in the same location in the image plane.

Shaped Aperture Masks

Shaped aperture masks are obstructions placed at telescope apertures that are machined into shapes that strategically diffract light away from discovery zones in the image. Standard circular apertures will produce interference patterns in the shape of Airy rings (Figure 8), but shaped apertures—whose forms are often generated using numerical methods—can yield complicated diffraction patterns that defy concise mathematical representation. Because the discovery zones are spared the vast majority of the light produced by the primary star, secondary stars should be easier to spot in these regions than they would be without a mask.

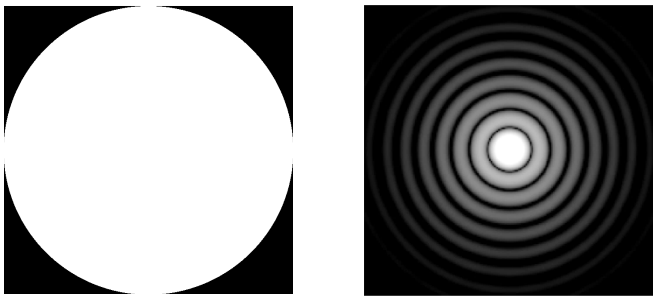

Figure 8. A simple circular aperture (left) and the Airy disc diffraction pattern it creates (right), plotted on a nonlinear brightness scale

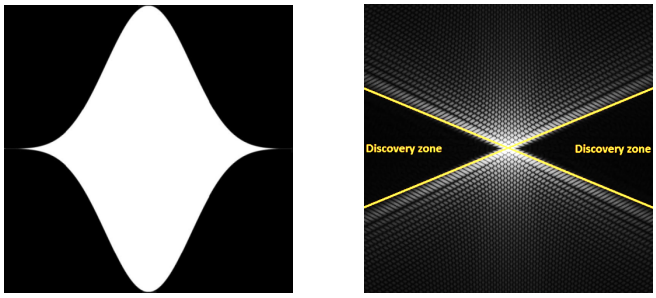

Figure 9. Left: A reproduction of a mask developed by Kasdin et al. (2003) based on the generalized prolate spheroidal wave function proposed as an apodization function by Slepian (1965). Right: The characteristic diffraction pattern, plotted on a nonlinear scale. The discovery zones are marked.

Figure 9 shows an aperture mask in the shape of a Gaussian curve reflected about the horizontal axis. This shape was derived by Kasdin et al. (2003) based on prior work by Slepian (1965).

The power spectrum is the diffraction pattern we would expect for a single, infinitesimally small point of concentrated light. When multiple points of light are imaged, a superposition of these diffraction patterns is visible in spatial agreement with the points of light themselves (see Figure 10). It is important to note that this superposition is not linear with respect to intensity because of the imaginary components of the original Fourier transform.

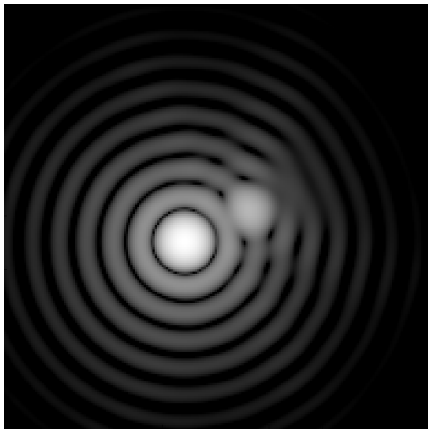

Figure 10. When imaging two points of light, the diffraction patterns superimpose themselves in the complex domain. This is a simulated Airy pattern formed by two nearby points of light at different brightnesses, shown on a nonlinear intensity scale.

In realistic usage conditions, the incoming light is not arranged into neat points but rather into distributed regions caused by atmospheric diffusion and other distortion effects. In this case, the convolution of the distributed regions with the nominal PSF will smear the output pattern. Thus, we cannot expect our mask-aided astronomical images to match the theoretical results perfectly. Only the more prominent features of the nominal pattern, such as the aforementioned discovery zones, will still be visible.

Telescope obstructions will cast their own diffraction patterns, so special care must be taken to avoid compromising a mask's beneficial effects. Consider a Gaussian mask applied to a telescope with a secondary mirror (Figure 11). The intended diffraction pattern of Figure 9 is present, but so too is the Airy pattern of Figure 8. The obstruction eliminates our discovery zones!

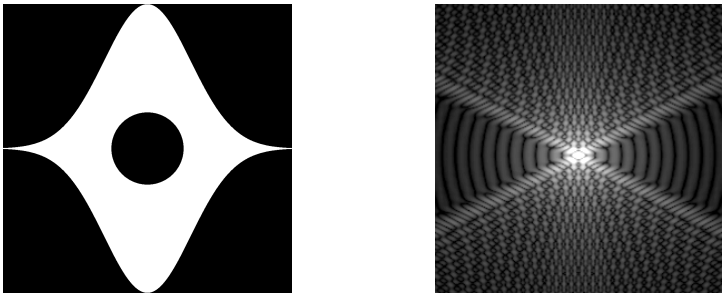

Figure 11. The combination of a Gaussian mask with an unaltered central obstruction (left) leads to an undesirable diffraction pattern (right), plotted on a nonlinear brightness scale.

There are at least two ways to address this problem. One might design a mask with multiple small apertures placed such that they do not overlap the central obstruction. Alternatively, one might reshape the obstruction by covering it with a shaped occulter that casts a similar diffraction pattern as the aperture itself (Figure 12). The throughput will be reduced, but more importantly, the diffraction pattern will retain its discovery zones. As mentioned in "History" below, Carlotti et al. (2011) present an optimal, though perhaps less intuitive, method of handling central obstructions.

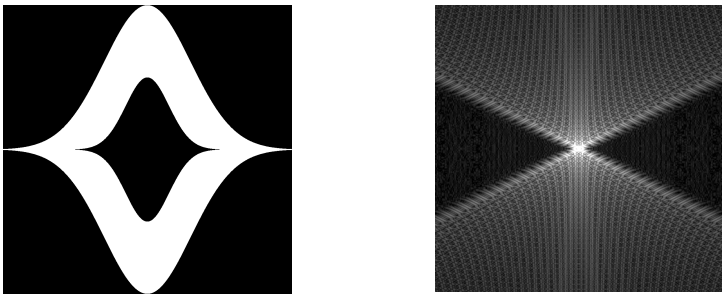

Figure 12. Covering the obstruction with a secondary Gaussian shape (left) restores a usable diffraction pattern (right), plotted on a nonlinear brightness scale.

History

The first aperture masks had simple geometries. In the 1830s, John Herschel used an equilateral triangular opening (Figure 13) to observe double stars while surveying the southern sky at the Cape of Good Hope (Herschel 1847). This shape tends to distribute points of light along six flanges of an image (Smith and Marsh 1974) and allows better visibility of faint companion stars. Edward Emerson Barnard built upon Herschel's work by developing a hexagonal mask (Figure 14) in the early 20th century that yields a similar six-flanged pattern (Sheehan 1995; Smith and Marsh 1974).

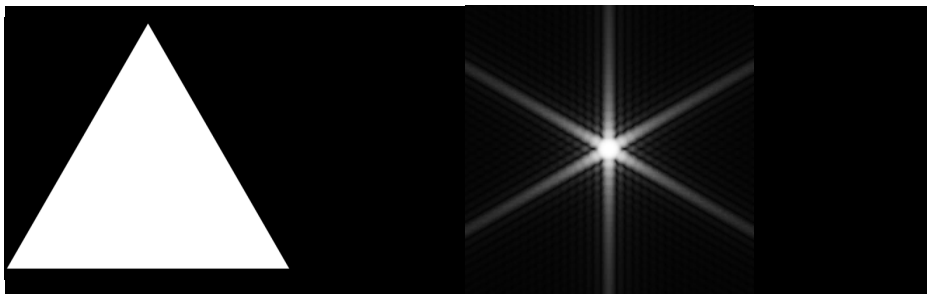

Figure 13. An equilateral triangle aperture (left) and its characteristic diffraction pattern (right), plotted on a nonlinear brightness scale.

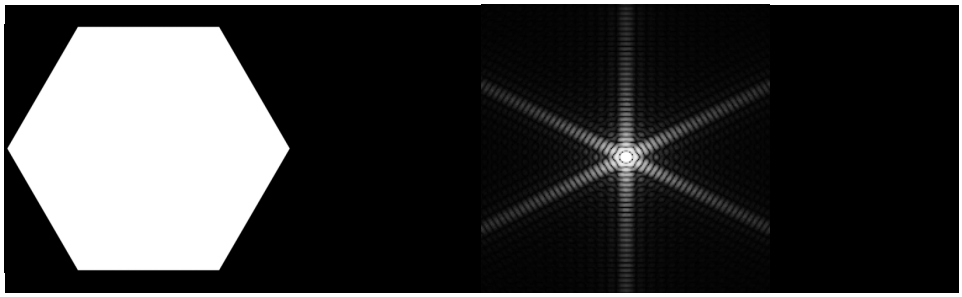

Figure 14. A regular hexagon aperture (left) and its characteristic diffraction pattern (right), plotted on a nonlinear brightness scale.

Mask designs advanced as the mathematics to describe wave interference advanced. David Slepian proposed a prolate spheroidal wave function as an apodization function in the 1960s (Slepian 1965). Unlike a shaped mask that uses a binary transmission profile, Slepian's apodizer had a transparency gradient, with some regions more opaque and others more transparent. Indeed, he never discussed a shaped pupil mask (Kasdin 2014). Only in the early 2000s did David Spergel and Jeremy Kasdin adapt Slepian's work into mask shapes such as the one in Figure 9.

Robert Vanderbei, Jeremy Kasdin, and David Spergel made further mask design advances in the early 2000s by using complex numerical techniques. Their masks, formed at the hands of mathematical theory, take on rather unusual shapes such as those seen in Figure 15 (Kasdin et al. 2003). Other proposed masks comprise concentric ring obstructions (Figure 16) (Vanderbei et al. 2003a) and intricate checkerboard patterns (Figure 17) (Vanderbei et al. 2004). Many of these complex masks would not be possible to manufacture with conventional construction methods due to their lack of full structural connectivity. Vanderbei, Kasdin, and Spergel recognized the construction difficulties (Kasdin et al. 2003) and developed a subset of masks following additional mathematical constraints to ensure their manufacturability (Vanderbei et al. 2003b).

Alexis Carlotti later joined Vanderbei and Kasdin to develop optimal apodization functions for masks to be used in the presence of arbitrary telescope obstructions and aperture shapes (Carlotti et al. 2011). Thus, even if some incoming light is blocked by a secondary mirror or a spider support structure, an optimal mask shape can still be calculated numerically. For example, Carlotti et al. (2011) derived an optimal mask for the unique mirror and support structure of the James Webb Space Telescope (Figure 18). The mask and its diffraction pattern are shown in Figure 19.

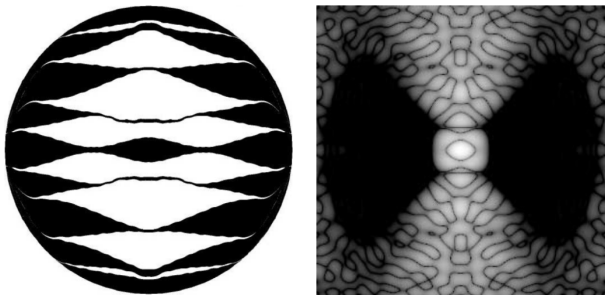

Figure 15. Left: One mask proposed by Kasdin et al. (2003). Some walls are thin, but the mask does have complete structural connectivity. Right: The mask's characteristic diffraction pattern (Kasdin et al. 2003), plotted on a nonlinear brightness scale. Note how the discovery zones are limited both by azimuth angle and radius.

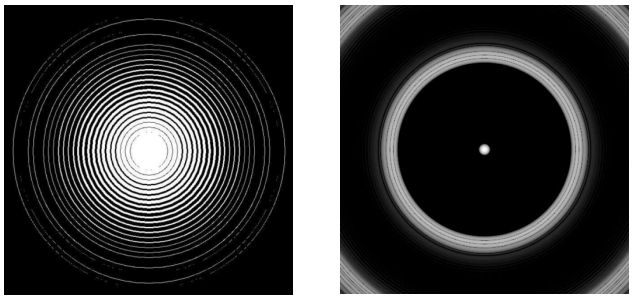

Figure 16. Left: A mask comprised of concentric annular openings (Vanderbei et al. 2003a). Right: The mask's characteristic diffraction pattern (Vanderbei et al. 2003a), plotted on a nonlinear brightness scale.
Note how the pattern is not azimuthally limited.

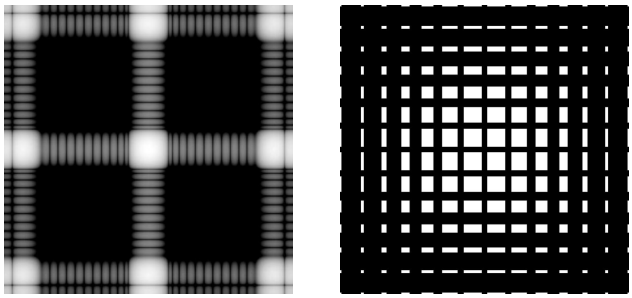

Figure 17. Left: A checkerboard mask (Vanderbei et al. 2004). Right: The mask's characteristic diffraction pattern (Vanderbei et al. 2004), plotted with a nonlinear brightness scale. The bright "struts" of the PSF intersect to form especially bright points, insulating the remaining square regions from light's influence.

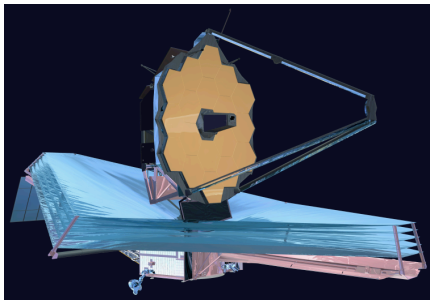

Figure 18. The James Webb Space Telescope (*NASA.gov*).

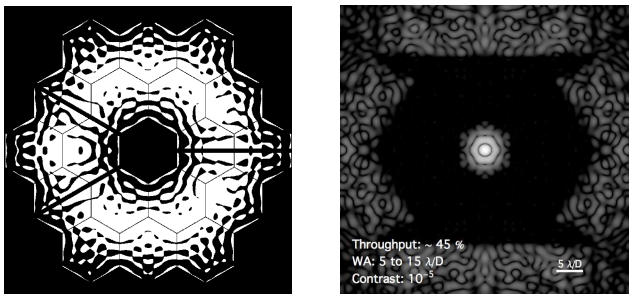

Figure 19. Left: A mask Carlotti et al. (2011) optimized for the James Webb Space Telescope of Figure 18. Note how the mask accounts for the hexagonal shapes in the primary mirror, the central obstruction caused by the secondary mirror, and the structure supporting the secondary. Right: The mask's characteristic diffraction pattern, plotted on a nonlinear intensity scale (Carlotti et al. 2011).

The aforementioned masks operate entirely on the amplitudes of the frequency components. Other scientists, including Rouan et al. (2000) and Haguenauer et al. (2006), have proposed phase masks that shift the phase of the incoming light to achieve a similar effect as the amplitude masks. While these phase-shift masks work very well in simulations, their physical realization presents fabrication challenges, typically involving the formation of a glass plate with a precise thickness profile. These challenges lead to a high cost.

Today, shaped masks are proposed for use in exoplanet discovery and observation, a field concerning delta magnitudes even more extreme than those of large-delta-magnitude close binary systems. The masks described above are designed for high contrast ratios ranging from 10^5 to 10^{10} and are "baselined for an upcoming mission" (Kasdin 2014).

Practical Usage

Masks influenced by Slepian (1965) and the subsequent developments by Vanderbei, Kasdin, and Spergel have already been used by a number of astronomers. Daley (2014) constructed a Gaussian mask (Figure 9) out of a manila folder affixed to plywood and combined it with a highly-attenuating occulting strip. His results for Sirius and its faint double—stars differing by 9.96 stellar magnitudes and separated by 9.66 arcseconds—are seen in Figure 20. Note how the secondary star is clearly seen in the discovery zone (rotated approximately 90 degrees from Figure 9) and how the occulting strip further reduces interference from the bright primary. The angular separation between the stars is larger than the seeing limit. Speckle interferometry techniques would have allowed even closer stars to be identified.

Debes et al. (2002) used a mask with multiple Gaussian apertures (Figure 21) to study binary stars, including μ Her A (Figure 22), with Mt. Wilson's 100-inch telescope. Debes et al. (2002) estimated the star separation of μ Her A as 1.3 ± 0.2 arcseconds. In prior observations, Turner et al. (2001) found the magnitude difference to be 9.29 in R-band and 7.26 in I-band.

These observations at Mt. Wilson were "the first attempt at high-contrast imaging with a [Gaussian aperture pupil mask]" (Debes et al. 2002). The group commented on the "relative ease and speed with which these first masks [were] produced" and described the technology as "promising," but they did acknowledge some difficulties, largely those caused by "imperfect atmospheric correction, scattered light in the telescope, and a diffuse thermal background" (Debes et al. 2002). Their mask's imperfect diffraction pattern is compared with the theoretical diffraction pattern in Figure 23.

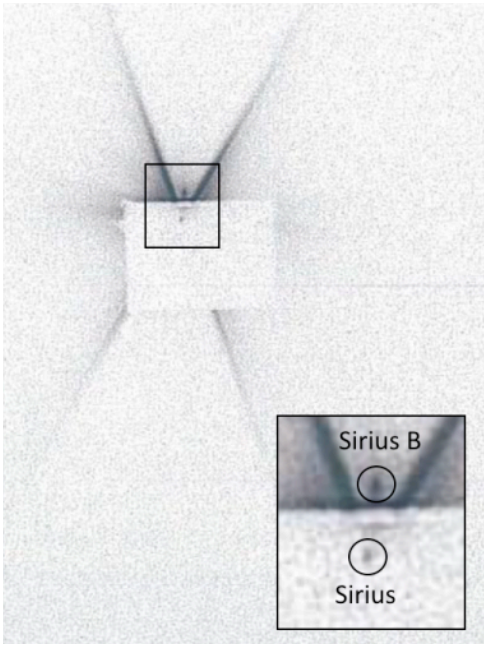

Figure 20. CCD image of AGC 1AB (Sirius) acquired by Daley (2014) using a shaped aperture mask of the design shown in Figure 9, coupled with a thin foil occulting strip. The image is black–white inverted and a portion has been copied and enlarged for clarity. The dot of light contained within the light rectangular region is the attenuated primary star (Sirius); the dot immediately above is the secondary (Sirius B).

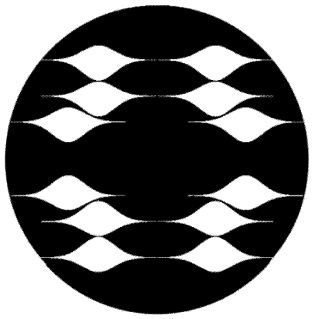

Figure 21. The mask used by Debes et al. (2002) on Mount Wilson's 100-inch telescope.

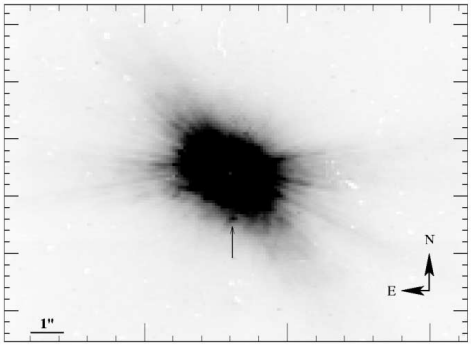

Figure 22. The result obtained by Debes et al. (2002) for μ Her A using the mask of Figure 21 at Mount Wilson's 100-inch telescope. A faint companion is visible at the small arrowhead toward the image's center.

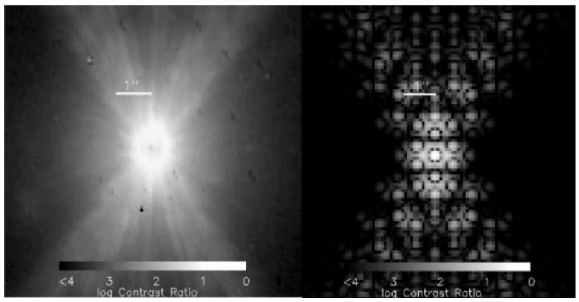

Figure 23. Obtained diffraction pattern (left) compared to theoretical diffraction pattern (right) for the observations performed by Debes et al. (2002) on ε Eridani. Intensity is plotted on a nonlinear scale.

The Mt. Wilson telescope has a secondary mirror and a structure to support it that both obstruct the optical path. Debes et al. (2002) used multiple Gaussian openings placed about the center of the telescope to avoid these obstructions. Debes and Ge demonstrated the merits of this Gaussian array approach over other possible configurations in a subsequent paper (Debes & Ge 2004).

Aperture Masks for a Schmidt–Cassegrain Telescope

Secondary mirrors are not unique to large telescopes. Consider the more modestly sized Celestron C11 Schmidt–Cassegrain telescope of Figure 24 which the authors will use to evaluate mask performance on smaller apertures. The circular obstruction caused by the secondary mirror accounts for over one third of the diameter of the primary mirror. Figure 25 shows the aperture shape and its default diffraction pattern. The PSF somewhat resembles an Airy disc because of the aperture's azimuthal symmetry.

Figure 24. The aperture of the Celestron C11 Schmidt–Cassegrain telescope. Note how the secondary mirror embedded in the corrector plate obstructs the aperture.

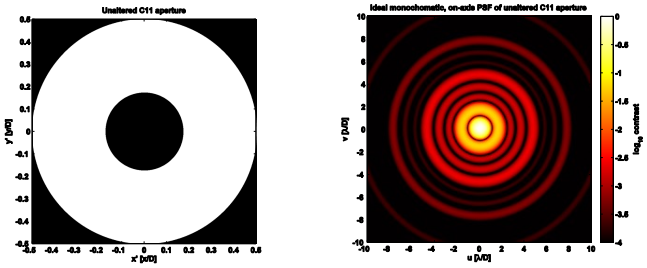

Figure 25. The unaltered C11 aperture (left) and its characteristic diffraction pattern (right), plotted on a nonlinear scale. Black regions have theoretical contrast ratios better than 10–4, equivalent to 10 stellar magnitudes.

Double Gaussian Mask

One simple mask design comprises a Gaussian outline with a Gaussian obstruction in the center akin to Figure 12. The central shape is just large enough to cover the secondary mirror cap. The mask's diffraction pattern, scaled to a small angular window, is seen in Figure 26.

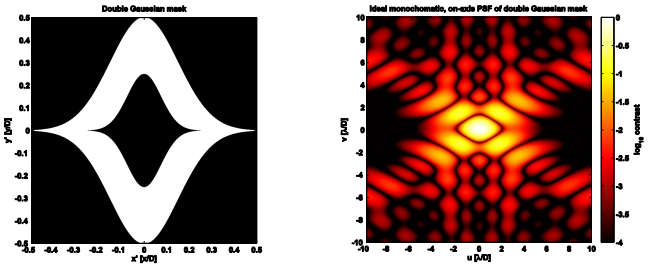

Figure 26. A Gaussian mask with a Gaussian obstruction large enough to cover the secondary mirror cap (left), and the mask's theoretical diffraction pattern (right), plotted on a nonlinear scale. Note the excellent contrast toward the left and right of the pattern.

This design achieves very deep contrast, but it does so at a relatively large angular distance from the center of the diffraction pattern. We would willingly sacrifice some contrast for a smaller inner working angle (IWA). For this, we resort to numerical optimization.

Optimization Overview

Based on the measurements by Foley, we start with an 11-inch circular telescope pupil with a 36% circular obstruction in the center. To be conservative with the alignment tolerance, we slightly oversize this obstruction. (The actual diameter ratio measured by Foley is $\frac{3.811\text{ in}}{11\text{ in}} = 0.346$.)

The project is aiming for contrast ratios between 7 and 6 astronomical magnitudes (equivalently, in base 10 logarithms the range is –2.8 to –2.4, and in terms of linear ratios, 630 to 250), and as small an inner working angle (IWA) as possible. For reference, observing at a wavelength of 550 nm with an 11-inch aperture, the λ/D diffraction width is

$$\frac{\lambda}{D} = \left(\frac{550\times10^{-9}\text{ m}}{11\text{ in}}\right)\left(\frac{1\text{ in}}{2.54\text{ cm}}\right)\left(\frac{100\text{ cm}}{1\text{ m}}\right)\left(\frac{360^\circ}{2\pi\text{ rad}}\right)\left(\frac{3600\text{ as}}{1^\circ}\right)$$

$$\rightarrow \boxed{\frac{\lambda}{D} = 0.406\text{ as}}$$

Also note, from here on out we describe contrast in base-10 logarithms, including the plots. There are two classes of shaped pupil solutions we explored. First, circular solutions that create full annular (360-degree) dark zones around the star (Vanderbei et al. 2003). Second, shaped pupils that create dark zones confined to symmetric bowtie-shaped wedges on opposite sides of the star PSF. The telescope pupil has two-fold symmetry (x and y). Therefore, for efficiency, the shaped pupil can be optimized on one quadrant of the image plane and retain the desired symmetry in the pupil (after Carlotti et al. 2013).

Circular (Concentric Ring) Solutions

Even for the modest contrast we aim for, we hit a wall trying to reach any circular solution with inner working angle below $2.4\,\lambda/D$. When we fix the inner working angle (IWA) to $2.4\,\lambda/D$ and the contrast constraint to 10^{-3} (deeper than the survey spec), we get the shaped pupil mask, PSF, and radial contrast cut shown in Figure 27. Note that in the mask diagram, the bright (yellow) pixels represent the transparent parts, while dark pixels are opaque.

We also plotted the radial contrast curve of the open C-11 aperture (open circle with 36% central obstruction) as a reference. It is evident that at angular separations above about $2.2\,\lambda/D$, the ideal telescope PSF is already meeting and exceeding the contrast spec of the binary star survey.

The circular mask optimization program has no trouble creating deep contrast above angular separation $2.4\,\lambda/D$. However, it remains to be seen whether seeing-limited speckle interferometry observations can take advantage of such large "ideal" wavefront contrast gains. This, combined with difficulty of fabricating two free-standing obstructing rings, make this type of mask difficult to recommend for the project.

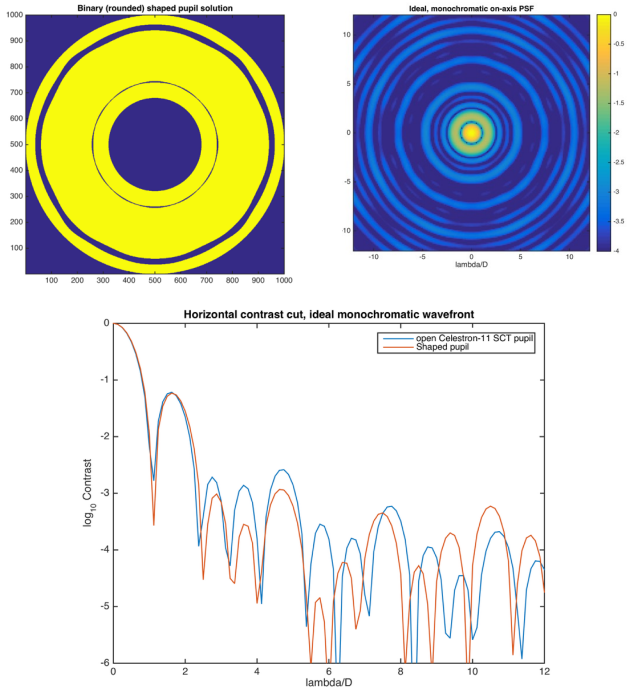

Figure 27. A concentric ring mask (top-left), its PSF (top-right), and a radial contrast cut (bottom).

Solutions with Bowtie-Shaped Search Zones

When the optimization program constrains the contrast only below some fixed polar angle in the image quadrant, the result is a mask with a bowtie-shaped search zone. With 90-degree wedges, by trial and error we found that the inner working angle has an absolute lower limit of $1.2\,\lambda/D$ (0.5 as at 550 nm). For a contrast goal of$10^{-2.7}$, the solution is simply two large obstructions. Each obstruction is connected to either the interior or exterior edges of the aperture. At larger contrasts, for example $10^{-3.0}$, the mask geometry becomes more complicated, with more free-standing islands, and the fraction of open area drops. In Figure 28, we show the shaped pupil solution, PSF, and horizontal contrast cut for the $1.2\,\lambda/D$ IWA, $10^{-2.7}$ contrast design.

As the contrast curve (measured in the horizontal cut extending from the center of the image) shows, this shaped pupil pushes down the first sidelobe of the ideal telescope PSF by over an order of magnitude. Therefore, it may offer a significant boost in the binary star target sample available to the telescope. The relatively simple mask layout is another compelling feature.

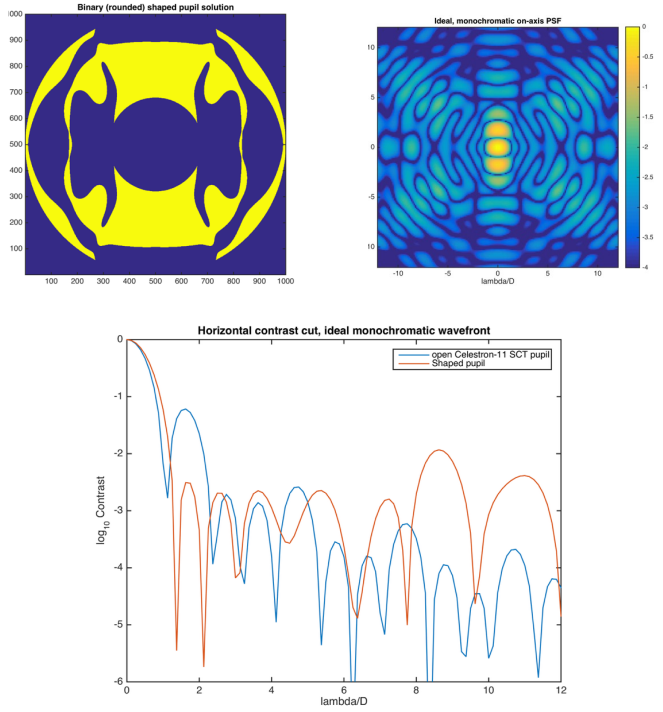

Figure 28. A bowtie mask (top-left), its PSF (top-right), and a horizontal contrast cut (bottom).

Considering its simple shape alongside its strong performance, the bowtie mask is a good choice to pursue alongside the double Gaussian mask. The double Gaussian mask has deep contrast but a large inner working angle; the bowtie mask has somewhat less contrast but a very small inner working angle. The two complement one another well and should elucidate whether contrast or inner working angle is easier to maintain in practice.

Testing

With two qualified mask designs, the next step is to construct the masks and perform basic tests to ensure the shaped-aperture approach is viable. The bowtie mask shows great promise in simulations, but we choose to begin with the double Gaussian mask because of its particularly distinctive hourglass-shaped diffraction pattern. The double Gaussian mask, cut out of 1/8-inch-thickness newsboard material with the aid of a laser cutter, is seen attached to the C11 in Figure 29. A beam had to be added across the center of the mask for structural contiguity. This beam contributes a vertical spike to the diffraction pattern.

Rowe simulated the results from this configuration with his Atmospheric Seeing Distortion program (ASD), which takes into account atmospheric phase distortion and camera sensitivity as it performs speckle interferometry on simulated images. Figure 30 shows the simulated autocorrelation result of a binary star system before and after the application of the double Gaussian mask.

Speckle interferometry contains an autocorrelation step that appears to form direct images of the stellar system, but this similarity is an illusion. The process duplicates the stars' combined diffraction pattern, producing bright points of light that outnumber the actual stars in view. Still, the angle and separation of stars can be determined—in this case, measured from the center of the image to one of the two bright points of light on the horizontal axis. These bright points are more distinct with the simulated mask than without it, making the measurement more robust and suggesting that the physical mask may improve practical measurements in a similar fashion.

Figure 29. The double Gaussian mask applied to the Celestron C11 telescope. The mask's outer gear teeth are designed to interface with an automatic rotation mechanism (not pictured).

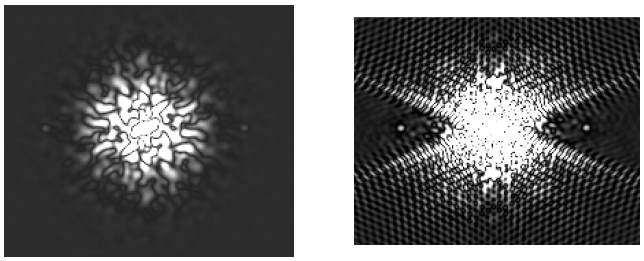

Figure 30. Rowe's simulated speckle interferometry results for a synthetic binary system viewed without a mask (left) and with a double Gaussian mask (right).

Jimmy Ray performed the double Gaussian mask's first test, in which he observed Rigel and its companion, Rigel B (Figure 31). The expected hourglass shape is quite visible, with notably dark discovery zones toward the image's left and right sides. The test confirms the mask's basic functionality.

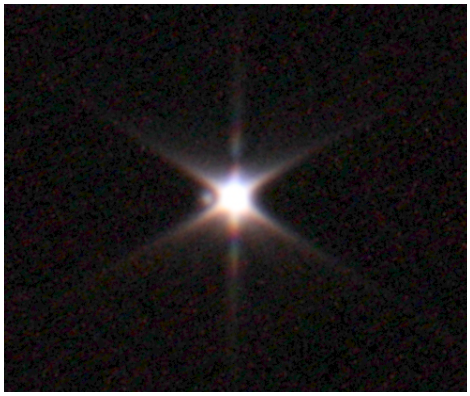

Figure 31. Rigel as captured by Ray using a double Gaussian mask. Rigel B, in Rigel's discovery zone, is visible just to the left of center. This image does not use speckle interferometry.

Rigel and Rigel B were an easy target because they were separated by 9 arcseconds. Future tests will explore the resolving capacity of the double Gaussian mask as well as the bowtie mask. We will use a CCD camera with speckle interferometry as we work toward progressively more challenging targets. It is our hope that these masks will prove to enhance the ability of small, ground-based telescopes to observe binary stars.

Acknowledgements

We wish to extend our thanks to Jimmy Ray for performing our astronomical testing and enthusiastically supporting the project; to Jeremy Kasdin for providing crucial feedback on an early version of this paper; to James Daley for sharing his hands-on experience with aperture masks; and to Robert Argyle for contributing sources that would otherwise be very hard to find. We also thank the faculty and staff of California Polytechnic State University for facilitating this research and supporting the scientific process through the University's "learn by doing" philosophy. Genet thanks California Polytechnic State University Office of Research and Economic Development for support through their Extramural Funding Initiative, and the W. M. Keck Foundation for support through the Concordia University Undergraduate Education Program. We all thank Vera Wallen for editorial suggestions.

References

2008. Andor Luca-S 658M specifications. *Andor Technology*.

Carlotti, A., Vanderbei, R., & Kasdin, J. 2011. Optimal pupil apodizations of arbitrary apertures for high-contrast imaging. *Journal of the Optical Society of America.*

Carlotti, A., Kasdin, J., Vanderbei, R., & Delorme, J. R. 2013. Optimized shaped pupil masks for pupil with obscuration. *Society of Photo-Optical Instrumentation Engineers (SPIE) Conference Series*, 8442.

2013. Cost estimate of the James Webb space telescope. NASA.gov.

Daley, J. 2014. LSO double star measures for the year 2012. *Journal of Double Star Observations*, 10, 136–138.

Debes, J., Ge, J., & Chakraborty, A. 2002. First high-contrast imaging using a Gaussian aperture pupil mask. *The Astrophysical Journal,* 572, L165–L168.

Debes, J. & Ge, J. 2004. High-contrast imaging with Gaussian aperture pupil masks. *Publications of the Astronomical Society of the Pacific*, 116(821), 674–681.

Dupuy, T., Liu, M., Bowler, B., Cushing, M., Helling, C., Witte, S., & Hauschildt, P. 2010. Studying the physical diversity of late-m dwarfs with dynamical masses. *The Astrophysical Journal*, 721(2), 1725–1747.

Haguenauer, P., Serabyn, E., Mennesson, B., Wallace, J., Gappinger, R., Troy, M., Bloemhof, E., Moore, J., & Koresko, C. 2006. Astronomical near-neighbor detection with a four-quadrant phase mask (FQPM) coronagraph. *SPIE Proceedings*, 62651G.

Hecht, E. 2002. *Optics*, 4. Reading, MA: Addison-Wesley, 540.

Herschel, J. 1847. Results of astronomical observations made during the years 1834, 5, 6, 7, 8, at the Cape of Good Hope; being the completion of a telescopic survey of the whole surface of the visible heavens, commenced in 1825. London: Elder Smith, 165.

2012. Hertzsprung–Russell diagram. *Encyclopaedia Britannica*.

Kasdin, J. 2014. Speckle, masks, and adaptive optics for large delta magnitudes. E-mail.

Kasdin, J., Vanderbei, R., Spergel, D., & Littman, M. 2003. Extrasolar planet finding via optimal apodized-pupil and shaped-pupil coronographs. *The Astrophysical Journal*, 582, 1147–1161.

Oppenheimer, B. 2003. Coronography, American Museum of Natural History.

Richmond, M. 2011. Continuous spectra. Rochester Institute of Technology. Web. Licensed under Creative Commons license CC BY-NC-SA 2.0.

Rouan, D., Riaud, P., Boccaletti, A., Clénet, Y., & Labeyrie, A. 2000. The four-quadrant phase-mask coronagraph. *Publications of the Astronomical Society of the Pacific*, 112, 777, 1479–1486.

Sheehan, W. 1995. Disappointments and triumphs. In *The Immortal Fire Within: The Life and Work of Edward Emerson Barnard.* Cambridge: Cambridge University Press, 347.

Sinnot, R. & Ashford, A. 2005. The martian moons in 2007–08. *Sky and Telescope.*

Sivaramakrishnan, A., Koresko, C., Makidon, R., Berkefeld, T., & Kuchner, M. 2001. Ground-based coronography with high-order adaptive optics. *The Astrophysical Journal*, 552, 397–408.

Slepian, D. 1965. Analytic solution of two apodization problems. *Journal of the Optical Society of America*, 55, 9, 1110–1114.

Smith, R. & Marsh, J. 1974. Diffraction patterns of simple apertures. *Journal of the Optical Society of America,* 64, 6, 798–803.

Turner, N., ten Brummelaar, T., McAlister, H., Mason, B., Hartkopf, W., & Roberts, L Jr. 2001. Search for faint companions to nearby solar-like stars using the adaptive optics system at Mount Wilson Observatory. *The Astronomical Journal,* 121, 3254–3258.

Vanderbei, R., Spergel, D., & Kasdin, J. 2003a. Spiderweb masks for high-contrast imaging. *The Astrophysical Journal,* 590, 593–603.

Vanderbei, R., Spergel, D., & Kasdin, J. 2003b. Circularly symmetric apodization via star-shaped masks. *The Astrophysical Journal*, 599, 686–694.
Vanderbei, R., Kasdin, J., & Spergel, D. 2004. Checkerboard-mask coronagraphs for high-contrast imaging. *The Astrophysical Journal*, 615, 555–561.